EXPERIMENTING ROTORCRAFT FLIGHT IN COMPLEX ENVIRONMENTAL CONDITIONS USING THE WIND TUNNEL: HELICOPTER SHIP LANDING CASE

Neda Taymourtash[1], Alex Zanotti[2], Giuseppe Gibertini[3] & Giuseppe Quaranta[4]

[1]Post-Doc. Researcher
[2]Assistant Professor
[3]Associate Professor
[4]Full Professor
[1,2,3,4]Department of Aerospace Science and Technology, Politecnico di Milano, Milan, Italy.

Abstract

This paper presents an experimental approach to study the aerodynamic loading of a scaled helicopter model while strongly affected by the environmental conditions. The landing scenario over the deck of a simplified ship geometry has been considered where the aerodynamic interaction between rotor inflow and ship airwake results in additional workload for the pilot. First, the flow field of the isolated-ship was studied by means of pressure measurements and Particle Image Velocimetry in various wind conditions. Then, the aerodynamic loads of the rotor was measured for a wide range of wind velocity, direction and position of the rotor over the deck. In addition to the time-averaged measurements, the frequency spectrum of the thrust and in-plane moments were obtained over the low-frequency range of interest for the flight mechanics and pilot workload. Furthermore, to understand the effect of the approach velocity, a fully dynamic landing maneuver was performed so that the results, in terms of unsteadiness of the aerodynamic loads, can be compared with the common approach of static way-points.

Keywords: wind tunnel test, helicopter, environmental effect, ship landing

1. Introduction

Search and rescue missions over land and water, urban transport, intervention in natural disasters, are examples of helicopter missions in which there is a strong interaction with the surrounding environment. In these situations, performance and handling qualities of the helicopter are highly affected by the presence of the obstacles in close proximity. Offshore operation is one of these tasks which requires a significantly increased level of workload from the pilots. Combination of the moving flight deck, unsteady profile of the environmental wind and flying very close to the superstructure of the ship results in a highly unsteady and turbulent flow field over the deck and consequently may endanger the safety of the operation [9]. To perform safety analysis, development of Helicopter-Ship Dynamic Interface (DI) simulation is found to be a promising alternative to the expensive and time-consuming at-sea flight trials [3]. Towards the development of high-fidelity DI simulation, airwake modeling is recognized as one of the crucial elements which can significantly affect the overall fidelity of the simulation. The importance of including the unsteady airwake, in addition to the steady components, was evaluated by performing piloted simulation to obtain the SHOL envelope [11]. In this regard, various numerical or experimental approaches can be taken for airwake modelling which result in different levels of simulation fidelity. Scaled wind tunnel testing is one of these approaches which could provide a reliable source of information to be used in both modeling and validation phase of DI simulation development.

The isolated-ship airwake has been extensively studied through both numerical and experimental approaches. Various ship geometries were reproduced for the purpose of scaled experiments with

different level of structural details [22, 12, 2]. However, few experimental setups have been developed to study the coupled environment where the aerodynamic interaction between helicopter and ship airwake can be evaluated in both steady and unsteady states. One of the first experimental investigations was done by Zan at Aerodynamic Laboratory, National Research Council of Canada [6]. A setup was developed to evaluate the unsteady side-force, yawing moment, and drag force applied on a rotor-less Sea King fuselage immersed in the turbulent airwake of CPF. To quantify the unsteady loading, Power Spectral Densities (PSD) were calculated from the time histories of the measured aerodynamic loads, and the square root of the integral over the bandwidth of 0.2 to 2 Hz was taken as the measure of unsteadiness. Across this frequency range, the magnitude of the spectrum represents a portion of the pilot workload associated with response to the airwake turbulence. Consequently, a reasonable correlation was found between RMS loading and pilot workload obtained from flight tests. The setup was further modified by adding a 1:50 scale rotor of Sea King to account for the effect of rotor downwash on the fuselage loading [7]. It was shown that in most cases the unsteady loading increased with the presence of the rotor downwash. Also, the level of unsteadiness at different positions over the deck and in different wind speeds was changed compared with the rotor-less case.

Another setup was designed and developed at the University of Liverpool, UK, by Wang et al. to measure the unsteady forces and moments imposed by the airwake of a generic ship on a 1:54 scale model of Merlin AW-101 helicopter [17]. The setup, specially designed for testing in a water tunnel, was used to simulate two Wind-Over-Deck (WOD) conditions, including headwind and wind coming with a direction of $45°$ from the starboard side, conventionally indicated as Green45, and the measurements were conducted at fixed positions along the flight path of a landing maneuver [4]. Time-averaged measurements identified a region of thrust deficit in headwind and a pressure wall in the $45°$ wind angle. The unsteady loading was also compared in terms of severity and showed higher RMS loading in Green45 and particularly through the lateral translation phase. The setup has been used also to investigate the potential benefits of aerodynamic modifications to the ship geometry [5]. Various modifications were proposed and many were found effective in reducing the RMS forces and moments. In particular, the promising design concepts were a side-flap and notch modification which both showed consistent improvements of 25-50% in unsteady loading.

More recently, a setup was developed at Politecnico di Milano to study the aerodynamic interaction between a scaled-helicopter model and Simple Frigate Shape 1, as a generic ship geometry [15, 16]. This paper provides a complete overview of the developed setup and the tests performed to study the aerodynamic interaction between helicopter and ship in a fully coupled environment.

Initially, a series of wind tunnel tests were performed to characterise the airwake of the isolated ship in different WOD conditions, with and without Atmospheric Boundary Layer (ABL), using Particle Image Velocimetry (PIV) technique. Then, the time-averaged aerodynamic loads of the rotor were measured, while the helicopter was placed in a series of points representative of a stern landing trajectory and a vertical descent over the landing spot. In that case, a rotor without a swashplate was used and the blades were rigidly attached to the hub with a fixed pitch angle, so no load trimming was allowed. Steady load measurements were performed in two WOD conditions, including headwind and Red30, where red indicates a wind coming from the port side, in addition to a no-wind test. Then, a second series of tests were conducted focused on the effect of ship airwake on the unsteady aerodynamic loads of the rotor in a wide range of wind speed and direction. Towards this goal, the setup has been substantially improved so that a landing trajectory can be simulated while trimming the rotor to obtain a specific set of aerodynamic loads. Three different wind directions were selected, including headwind, Red30, and Red60. Furthermore, the tests in HW and Red30 were performed at two different wind speeds for each direction. Moreover, the new setup was exploited to simulate "Dynamic Landing" by setting a constant approach velocity for the helicopter to perform the landing maneuver.

In the following sections, first the details of the setup and instrumentation are introduced. Then, the procedure of the test divided in three main parts, will be explained. Finally, the results of each part will be presented and discussed.

2. Experimental Setup

The experiments were conducted in the large test chamber of the GVPM (Galleria del Vento Politecnico di Milano) with 13.84 m wide, 3.84 m high and length of 35 m. The test rig consists of a 4-bladed helicopter and a simplified ship model. The helicopter model was held by a horizontal strut fixed to a system of two motorised orthogonal sliding guides which was able to change the relative position of the helicopter with respect to the ship in both vertical and longitudinal directions. The whole setup was mounted on the large turning table of the test section with a diameter of 13 m, so that the effect of wind direction could be tested as well.

2.1 Ship Model

The generic frigate model selected for this study is a 1:12.5-scale model of Simple Frigate Shape 1 (SFS1) [19]. This geometry consists of a rectangular prism with a step on its rear and another prism on top which is acting like chimney over the ship superstructure. The flight deck and hangar wall were equipped with 77 and 35 pressure taps, respectively. The pressure measurements were performed using four low-range 32-ports pressure scanners embedded inside the ship model. The declared accuracy of the pressure scanners led to an estimated uncertainty for the pressure coefficient of approximately 0.15. Moreover, five high-frequency response Kulite transducers were placed along the longitudinal center line of the flight deck in order to measure the unsteady pressure. Pressures were acquired with a sampling frequency of 25000 Hz for a duration of 20 seconds in the isolated ship tests and 5 seconds while testing with the rotor over the deck. Figure 1 represents the geometry of the ship model with the layout of the pressure taps and Kulite transducers. Position of the Kulite transducers in ship reference frame is given in Table 1.

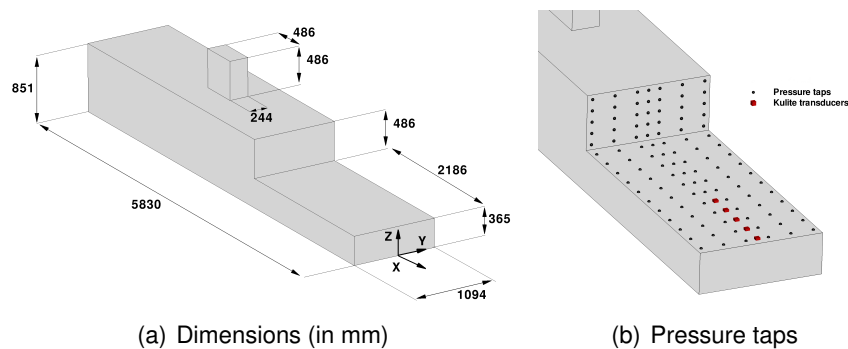(a) Dimensions (in mm)   (b) Pressure taps

Figure 1 – 1:12.5-scale model of SFS1 equipped with pressure taps and Kulite transducers.

Table 1 – Position of the Kulite transducers on the flight deck in ship reference frame.

Kulite Number	X [mm]	Y [mm]	Z [mm]
Kulite 1	-80	0	365
Kulite 2	-280	0	365
Kulite 3	-480	0	365
Kulite 4	-680	0	365
Kulite 5	-880	0	365

2.2 Helicopter Model

The helicopter model consists of a fuselage and a rotor with four untwisted and untapered rectangular blades, made of carbon-fiber composite materials with NACA0012 airfoil. In the first test campaign, a rigid hub without hinges was adopted, meaning that the blades were rigidly connected to the hub with a very stiff connector and a constant pitch angle of $10°$, while in the second campaign, a complete swashplate mechanism was implemented so that collective and cyclic commands could be applied to the blades to trim the aerodynamic loads. A six-components strain gauge balance was mounted

inside the fuselage to measure the aerodynamic loads acting on the rotor with a sampling frequency of 100 Hz. The rotor rotational speed was maintained in all tests by means of a brushless, low-voltage, electrical motor with an electric controller. A Hall-effect sensor giving the one per revolution signal was used in the first model as a feedback signal for RPM control. In the second campaign, an Electronic Speed Controller (ESC) was connected to the motor to record the angular speed with the same sampling frequency as the balance loads so that the load coefficients can be calculated based on instantaneous RPM of the rotor.

2.3 Scaling Parameter

The main scaling parameter applied to this investigation is to maintain the Strouhal number (advance ratio) of the full scale model. This matching requires the correct scaling of three parameters, including angular speed, geometry and free stream velocity. Considering Bo105 as a generic medium size helicopter, the geometric scale of each helicopter model is fixed based on the rotor radius. The rotational speed of the rotor was selected high enough to increase the Reynolds and Mach numbers, while reaching the desired advance ratio within the limits of free stream velocity of the wind tunnel test section. Parameters selected for each model are listed in the following table in comparison with Bo105.

Table 2 – Parameters of the wind tunnel helicopter models and Bo105.

Characteristic	WT-750	WT-970	Bo105
Number of Blades	4	4	4
Rotor Radius (m)	0.375	0.485	4.9
Angular Speed (rad/s)	270	211	44.4
Blade Chord (m)	0.032	0.042	0.27
Free Stream Velocity (m/s)	4.76	4.8-8.4	10.3-18
Advance Ratio	0.047	0.047-0.082	0.047-0.082
Tip Mach Number	0.3	0.3	0.63
Tip Reynolds Number	$2.2e5$	$2.2e5$	$3.9e6$

2.4 PIV Setup

The PIV system comprised a Litron NANO-L-200-15 Nd:Yag double-pulse laser with an output energy of 200 mJ and wavelength of 532 nm, and two Imperx ICL-B1921M CCD cameras with a 12-bit, 1952×1112 pixel array in tandem configuration. Each camera was equipped with a NIKKOR 50-mm lens. The laser was positioned on a suitable strut downstream of the ship model, so that the laser sheet was aligned with the X–Z plane. The laser was mounted on a longitudinal traversing system in order to cover the whole area of investigation along the deck providing the same light power. The cameras line of sight was aligned perpendicular to the laser sheet. The area of investigation of the first test campaign covered the whole shipdeck (more than 2 m × 0.5 m), thus, in order to achieve a better resolution of the image pairs, the measurement area included 10 multiple adjacent windows of 480 mm × 270 mm with a small overlapping among them. In the second campaign, two adjacent windows with the same dimensions of the previous tests, and with a small overlapping among them were surveyed to cover the longitudinal plane of the whole rotor disk for inflow investigation. In particular, the fore region of the disk was prioritised in the surveys in order to obtain more information on the rotor inflow. To avoid laser reflection over the blades during those tests, the closest line of the PIV area of investigation to the rotor was 48 mm above the disk plane. The data measured over this line were considered to extract the normal velocity along the longitudinal symmetry axis of the rotor. The position of the PIV measurement area along the deck and above the rotor is shown in Fig. 2.

2.5 Atmospheric Boundary Layer

The large test chamber of GVPM is equipped with several devices allowing the production of different velocity profiles with a wide range of turbulence intensities. For the purpose of ship airwake studies, two different free stream velocity profiles were considered: Smooth Flow (SF), in which there
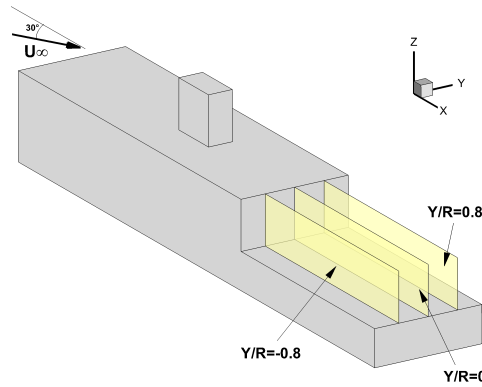
Figure 2 – Position of the PIV investigation planes.

were no upstream turbulators and so a uniform free stream velocity profile was generated, and the Atmospheric Boundary Layer (ABL), where turbulators were inserted upstream of the ship to obtain a velocity profile corresponding to the well-known power law model:

$$\frac{u}{u_{\text{ref}}} = \left(\frac{z}{z_{\text{ref}}} \right)^{\alpha} \tag{1}$$

where u is the mean velocity at height z, u_{ref} is the reference velocity measured at height z_{ref} and α is an exponent that depends on the roughness of the terrain. The ABL velocity profile generated in this experiment corresponds to the wind profile with $\alpha = 0.1$ which is suggested by Simiu et al. [13] for coastal areas. The wind tunnel free stream velocity for each test run was set using a Pitot probe placed above the ship superstructure. This choice was driven by the fact that anemometers are usually placed on ship's mast to be less affected by the ship airwake. In this experiment, the probe was positioned 180 mm above and 90 mm upstream of the top superstructure. For the tests with red-wind, i.e. wind coming from the port side of the ship, the Pitot probe was adjusted in order to have the static port in the same position as the head-wind test. As represented in Fig. 3, comparison of the ABL with the profile calculated by power law model shows a good agreement up to the reference height. Also, the profile of longitudinal turbulence intensity shows that ABL will significantly increase the turbulence intensity compared with SF. For instance, at height of the flight deck the turbulence intensity is increased from 2% in SF to 10% in ABL.
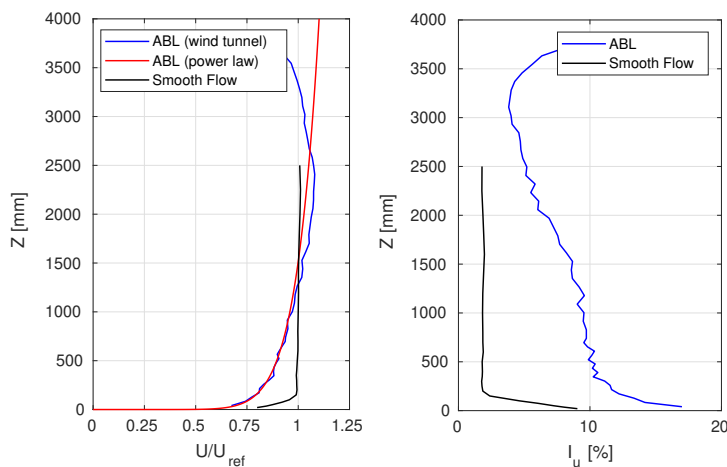

Figure 3 – Comparison of the mean velocity profile (left) and turbulence intensity (right) for ABL and Smooth Flow.

3. Test Plan

The tests presented here are divided in three main parts. In the following, the objectives, parameters and test conditions for each part will be introduced. Then, the results of these three parts will be presented and discussed separately in the next section.

3.1 Isolated-Ship Test

The first part is focused on the characterization of the flow field on the flight deck of the isolated-ship, i.e without presence of the helicopter model over the deck. The main objective is to assess the topology of the flow field over the flight deck with respect to three parameters: free stream velocity, wind direction and effect of the presence of the ABL. To this aim, PIV measurements along with unsteady pressure measured by Kulite sensors will be presented and discussed in the next section.

3.2 Helicopter-Ship Interaction: Steady Test

In this part, the effect of ship airwake on the inflow of the rotor and its aerodynamic loading has been studied while performing a landing maneuver. To simulate the landing maneuver, the helicopter model (WT-750) was positioned in a series of points representative of a typical stern landing trajectory. The trajectory, as shown in Fig. 4(a), consists of five points (P1 to P5) that can be divided into two distinctive segments: the initial phase in which the helicopter approaches the flight deck from the stern side along the center line of the flight deck, followed by a descent phase, i.e. an oblique path towards the landing point, which is considered close to the center of the flight deck. Furthermore, three additional points above the landing point were selected to simulate a vertical descent (P5 to P8). Since the rotor of WT-750 helicopter model could not be trimmed, this test was performed at the lowest free stream velocity (refer to Table 3), however from two different directions including headwind and Red30. It should be mentioned that aerodynamic loads presented in this part are the mean value of 5 seconds acquisition of the load cell repeated twice at each point. Consequently, the results of this part will show the effect of ship airwake on the steady loads, while the unsteady assessment will be the objective of the next part.

(a) Test points with first helicopter model (WT - 750)
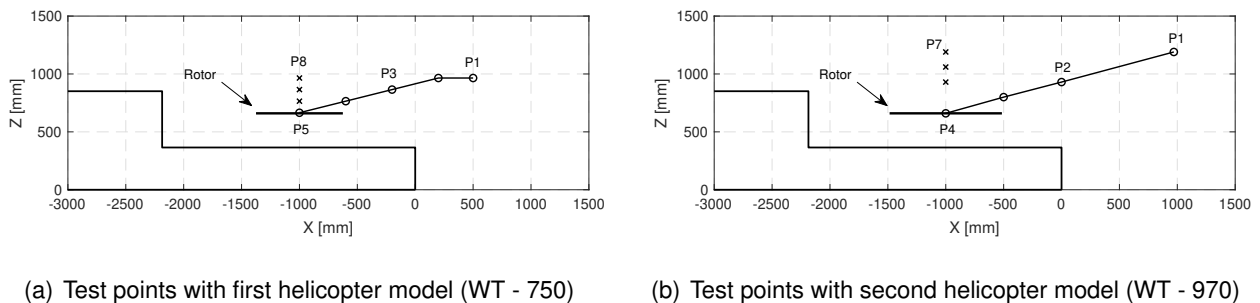
(b) Test points with second helicopter model (WT - 970)

Figure 4 – Side-view of the landing trajectory. Circles and crosses represent the position of the rotor center, respectively in the stern landing and vertical descent.

3.3 Helicopter-Ship Interaction: Unsteady Test

In this part, another stern landing trajectory was defined which includes four points (P1 to P4) along a descent path with a slope angle of $15°$ towards the landing point. Similarly, three additional points (P5 to P7) were selected which are representative of a vertical descent over the deck (Fig 4(b)). In these tests, after placing the rotor at each point, the rotor was trimmed to obtain a specific level of thrust and zero in-plane moments, by applying collective and cyclic commands. Then, trim commands were fixed and the acquisition of the loads was performed for 30 seconds with the sampling frequency of 100 Hz and repeated twice for each point. Taking advantage of trimming capability, the tests were performed in higher wind speeds as well. Five wind conditions were tested, including two velocities in headwind, two velocities in Red30, and one velocity in Red60.

Finally, a second approach called "Dynamic Landing", was tested in three wind conditions to study the effect of approach velocity of the helicopter on the unsteady loads. In this approach, the helicopter is moving towards the landing point with a constant velocity, while the trim controls, obtained during the static tests for each point, are applied to the rotor. The predefined trajectory, starts with 5 seconds initial hover at P1, after descending towards P4 with a constant velocity of 0.1 m/s, it ends with 5 seconds hover at P4. Regarding the scaling parameters of the test, the selected approach velocity corresponds to a velocity of 1 m/s with respect to the ship deck in full-scale, which is well representative of the final phase of a landing maneuver that is a low speed forward flight near the deck.

Table 3 – Longitudinal and vertical coordinates of the test points in ship reference frame (in mm).

Test Points	WT-750	WT-970
P1	[500 , 965]	[970 , 1190]
P2	[200 , 965]	[0 , 930]
P3	[-200, 865]	[-500 , 800]
P4	[-600 , 765]	[-1000 , 660]
P5	[-1000 , 665]	[-1000 , 930]
P6	[-1000 , 765]	[-1000 , 1060]
P7	[-1000 , 865]	[-1000 , 1190]
P8	[-1000 , 965]	-

4. Results and Discussion

In this section, the results of the above mentioned tests are presented and discussed separately within the three following sections.

4.1 Ship Airwake Analysis

Figure 5 compares the PIV measurements of the symmetry plane of the deck for two free stream velocities. In both conditions, the topology of the flow field over the deck is the one commonly seen downstream of a three dimensional backward facing step [10]. The flow field can be decomposed into three main zones: recirculation, reattachment and redeveloping regions as observed in [14]. Regarding the sharp edges of the ship model, the recirculation zone occurs immediately behind the hangar wall and reattaches about half-way along the flight deck. The airwake is directed downward over the recirculation zone, reflecting the fact that streamlines are bending towards the region of low pressure. The comparison between Fig. 5(a) and Fig. 5(b) shows that the structure of the flow field does not change by increasing the Reynolds number, as shown in other studies [21, 8]. As a matter of fact, the minimum ship-based Reynolds number of 3.5×10^5 is high enough to create a turbulent flow field and have a flow topology mainly driven by the presence of the sharp edges of the ship.

(a) $\beta = 0°$ - $U_\infty = 4.8$ m/s
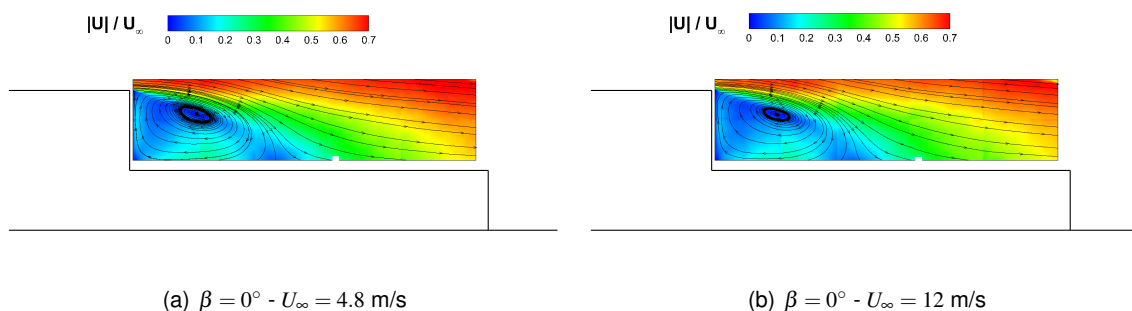
(b) $\beta = 0°$ - $U_\infty = 12$ m/s

Figure 5 – Contours of normalized in-plane velocity magnitude and streamlines in the symmetry plane.

To demonstrate the effect of wind direction, PIV measurements of the ship airwake in Red30 wind condition are presented in Fig. 6. Compared to Fig. 5(a), it can be seen that the size of the recirculation zone on the symmetry plane becomes larger when the wind is blowing from Red30, extending the area interested by the vortex in the upper part of the deck. However, the position of the reattachment point is not affected significantly. In this case, almost half of the flight deck is covered by a significantly lower-than-free stream-velocity region which may particularly affect the loading of the rotor and pilot activities during shipboard operations. In the port side plane, the recirculation region starts to develop close to edge of the hangar, while most of the deck remains unaffected, since in this region the air does not flow past the hangar step before arriving to the deck. Moving starboard, the recirculation region increases in size and thus the portion of the ship deck interested by low-speed flow increases as well. Consequently, it is possible to say that the symmetry of the horseshoe vortex created behind the hangar wall, whose topology is shown in [1], is clearly lost when the wind blows from the side, with the vortex core position that seems to drop only on the starboard side.

(a) $\beta = 30°$ - Symmetry plane

(b) $\beta = 30°$ - Port side plane
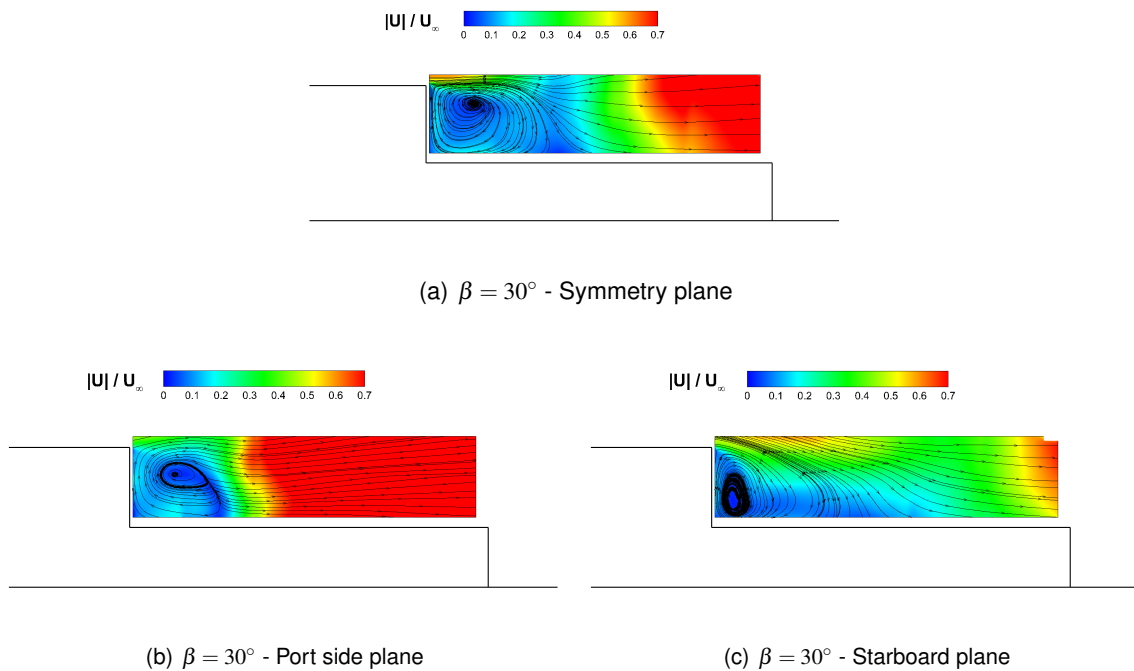

(c) $\beta = 30°$ - Starboard plane

Figure 6 – Contours of normalized in-plane velocity magnitude and streamlines in the symmetry plane, $U_\infty = 4.8$ m/s.

To quantify the effects of the presence of the ABL on the flow field a specific test with turbulators upstream of the ship was performed. Fig. 10 compares the airwake velocity measured on the symmetry plane with SF and ABL in headwind condition. Looking at time-averaged velocities, the airwake structure is very similar. This is further confirmed by the comparison of the pressure coefficient distribution on the deck.

As mentioned before, in the isolated-ship tests, pressure measurement was performed for a duration of 20 seconds. So, high frequency response of Kulite transducers can be used to evaluate the effect of different test parameters on the unsteady part of the ship airwake. To convert the recorded time-histories to the frequency domain, Welch's algorithm has been implemented. Welch's method computes an estimate of the power spectral density by dividing the data into overlapping segments, computing a modified periodogram for each segment and averaging the periodograms [18]. The windowing of each individual segment results in reducing the noise in the spectral density estimate, at the expense of frequency resolution. Here, the time histories are divided into 15 segments, each with 2^{15} data points and the Hamming window of equal length is used with 50% overlap between segments.

Figure 8 shows the power spectral densities of the pressure coefficients, measured by five Kulite transducers in two test conditions, HW and Red30. Regarding the position of the Kulite sensors, it
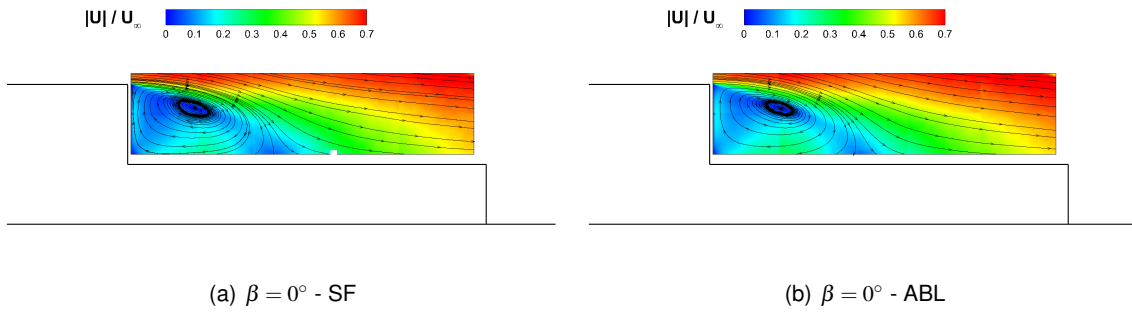
(a) $\beta = 0°$ - SF

(b) $\beta = 0°$ - ABL

Figure 7 – Contours of normalized in-plane velocity magnitude and streamlines in the symmetry plane, $U_\infty = 4.8$ m/s.

should be reminded that Kulite 1 is the closest to the stern edge and Kulite 5 is the closest one to the center of the deck (refer to Fig. 1 and Table 1 for the coordinates of Kulite sensors).
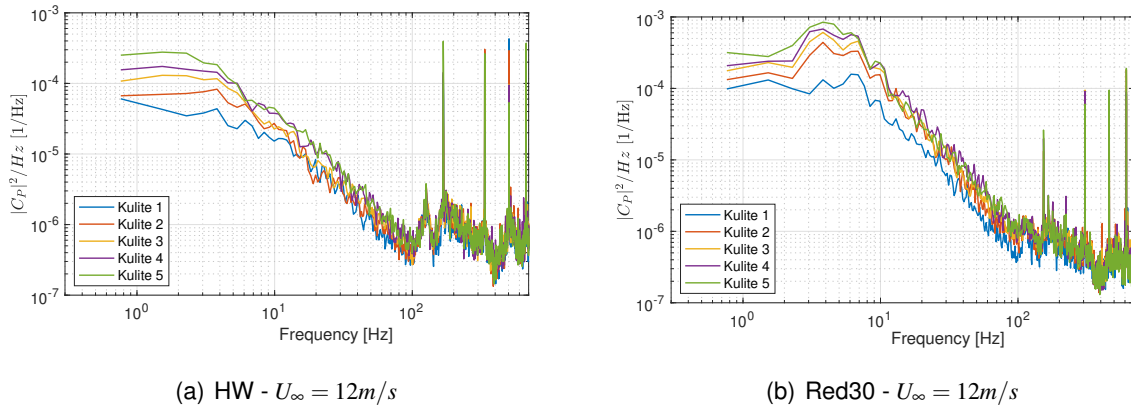

(a) HW - $U_\infty = 12m/s$

(b) Red30 - $U_\infty = 12m/s$

Figure 8 – Power spectral densities of pressure coefficient in HW and Red30.

It can be seen that in both test conditions, the energy of the spectrum is increasing from Kulite 1 towards Kulite 5, meaning that the unsteadiness of the airwake, especially over the lower-frequency range, is increasing towards the center of the deck. This could be expected regarding the PIV results previously presented, since closer to the center, the airwake is more affected by the highly-turbulent zone generated behind the hangar wall. Furthermore, the unsteadiness of two wind conditions can be compared for each Kulite measurement. To this aim, first a relevant range of frequency in full-scale model is mapped into the frequency scale of the experiment using the scaling parameters introduced in Table 3. Then, the energy of the spectrum should be calculated over this bandwidth of interest. Regarding the effect of the airwake turbulence on the pilot activities, the range of 0.2 up to 2 Hz in full-scale is considered relevant which corresponds to the range of 1.2 up to 12.1 Hz. Figure 9 compares the unsteadiness obtained over this range for all five Kulite sensors in two tested wind directions. It can be seen that with the wind coming from the port-side, the unsteadiness is significantly increased in all Kulite positions. This implies that the amount workload required from pilot in response to the turbulence of the airwake will be notably higher in Red30 compared to HW condition.

Comparing the PIV measurements, it was already shown that the presence of the ABL does not affect the mean flow field over the deck, however, to understand the effect on the unsteady airwake, time-resolved PIV should be performed. Alternatively, the frequency response of the Kulite sensors can be used to compare the unsteady pressure with and without presence of the ABL. Figure 10 shows the PSD of pressure coefficient measured by Kulite 1 in two wind directions. It can be seen that while in each wind direction, the PSDs follow the same trend with and without ABL, the increase of unsteadiness due to the presence of ABL profile becomes evident only in Red30 test condition. This is related to the fact that in headwind the turbulence caused by the interaction of the free stream
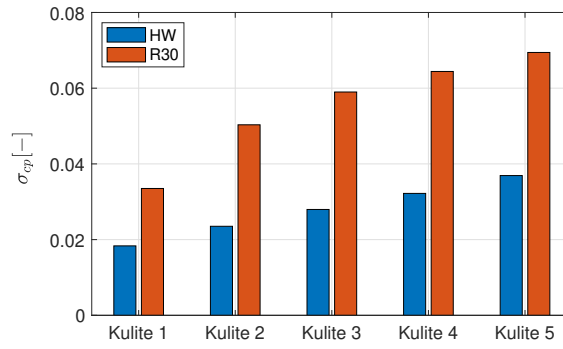
Figure 9 – Effect of wind direction on the unsteady pressure - Comparison of HW and Red30.

(a) HW - $U_\infty = 12m/s$
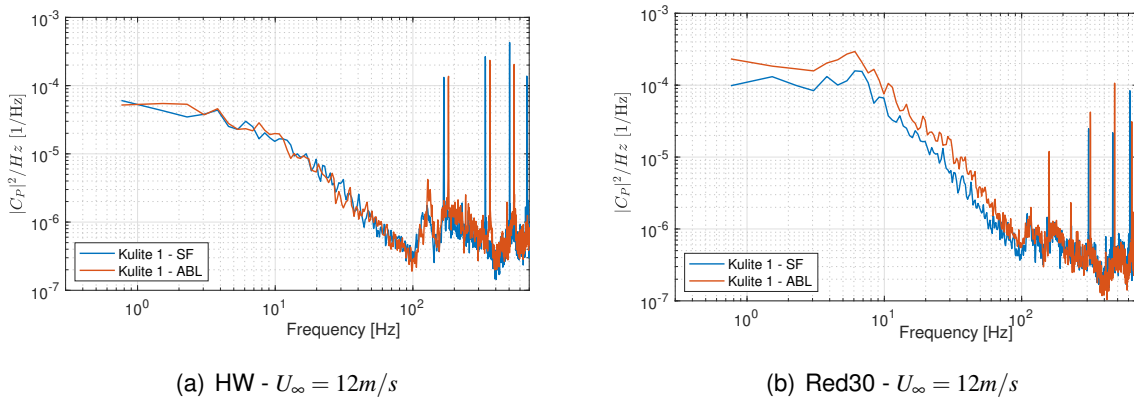

(b) Red30 - $U_\infty = 12m/s$

Figure 10 – Power spectral densities of pressure coefficient in HW and R30 - Comparison of SF and ABL tests.

with the superstructure and sharp edges of the hangar wall is the dominant effect and the additional turbulence of ABL profile does not increase the unsteadiness. However, with non-zero wind angle, the free stream passes over a part of the deck, especially near the stern side, without interaction with ship superstructure. This is the area where the effect of additional turbulence in ABL profile is expected to affect the flow field. To better quantify this effect for all Kulite positions, Fig. 11 shows the unsteadiness over the same bandwidth, as introduced before. The results confirm that in all five positions, the effect of ABL remains negligible in HW and will increase the unsteadiness of the flow field in Red30.
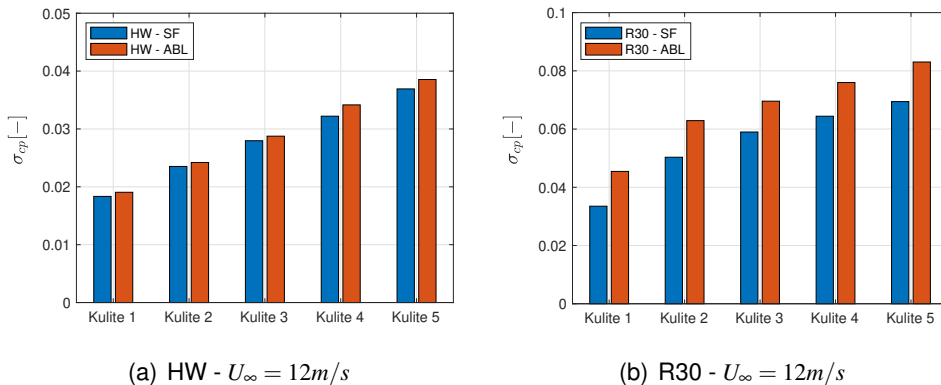

(a) HW - $U_\infty = 12m/s$

(b) R30 - $U_\infty = 12m/s$

Figure 11 – Effect of ABL on unsteady pressure at different Kulite positions - Comparison of SF and ABL tests.

10

4.2 Ship-Helicopter Interaction: Steady Measurements

As mentioned before, the objective of this part is studying the effect of ship airwake on the mean rotor loads while performing a landing test. Figure 12 presents the variation of thrust and in-plane moments for both stern landing and vertical descent in three test conditions. It should be noted that thrust and moment coefficients are normalized with respect to thrust and torque coefficients, measured in OGE condition which are $CT_{OGE} = 7.28 \times 10^{-3}$ and $CQ_{OGE} = 7.74 \times 10^{-4}$ respectively. It should be noted that the results are presented in rotor reference frame, with x axis from nose to tail, z axis bottom to top and y axis towards starboard. As shown in Fig. 12(a), thrust is increasing as the helicopter approaches the landing point, due to the ground effect induced by the ship deck. The thrust variation is more significant in hover (wind-off) condition, where an increase of about 15% of the OGE value is obtained at the landing point for the stern landing. The same behaviour can be observed in vertical landing as well. However, the ground effect is less intense with respect to the stern landing at the same height, when considering the wind-off case. For instance, in hover when the helicopter is placed in P6 ($X = -1000$ mm, $Z - Z_{\text{DECK}} = 400$ mm), the rotor experiences only 8% increase in thrust with respect to 10% in P4 ($X = -600$ mm, $Z - Z_{\text{DECK}} = 400$ mm), which is at the same height but farther from the hangar wall. This small difference is caused by the development of a recirculation region between the hangar wall and the helicopter [20], which consists of the fore part of the rotor wake that is deflected by the ship deck and the hangar wall and then re-ingested into the rotor. This causes a slightly increased induced velocity on the fore part of the rotor, together with the consequent thrust loss and a small nose-down (negative) variation of pitch moment particularly apparent for the vertical descent as the helicopter is moved downwards (see Fig.12(d)). For the stern landing at point P3, the slight peak of the pitching moment can be due to the non-symmetrical ground effect as the rotor disk is only partially inside the flight deck (see Fig. 12(c)). Concerning the roll moment, variations are more limited but a general trend to decrease its value moving toward the flight deck is recognizable for both landing trajectories.

For headwind tests, it can be appreciated that the beneficial effect due to ground is mitigated with respect to hover as can be seen in Figs. 12(a) and 12(a) for both stern landing and the lowermost position of the vertical descent. Furthermore, in the first point (P1) where the helicopter is totally outside of the ship airwake, a large pitch moment is generated by the rotor due to the influence of the external wind on the fixed rotor. As expected, this behaviour is mainly related to the non-symmetrical induced velocity distribution that is larger in the rear part of the rotor disk as the rotor wake is moving backward. This effect is obviously reduced when the helicopter is in the ship airwake and the horizontal velocity results to be lower, implying significant negative variations of the pitch moment can be appreciated while the helicopter enters the airwake of the ship, about 60% and 45% in stern landing and vertical descent, respectively. Another possible contribution to this is the downwash produced by the recirculation behind the hangar wall on the fore part of the disk that is larger when the helicopter is closer to the flight deck.

For the R30 tests, the beneficial effect due to ground is more mitigated than in headwind. In particular, about 7% of thrust reduction is observed with respect to hover test when the rotorcraft is placed at landing spot (see Figs. 15(a) and 15(b)). This is even more accentuated during the vertical descent, particularly at P8 in which the thrust reaches a value lower than in OGE condition (Fig. 12(b)). Looking at the moment coefficients the most apparent effect with respect to the headwind condition is related to the roll moment, whereas the trend of the pitch moment is quite similar. This could be mainly explained considering the effect of the free stream on induced velocity distribution on the rotor disk as already mentioned for the headwind condition. Indeed, in this case the non-symmetrical distribution from windward to lee side of the rotor disk produces an aerodynamic moment contribution that projected along the longitudinal axis of the helicopter results in a large negative roll moment, as can be seen in Figs. 12(e) and 12(f). This effect is reduced approaching the flight deck due to the reduction of the horizontal velocity, explaining the positive variations of the roll moment measured along both the landing trajectories.
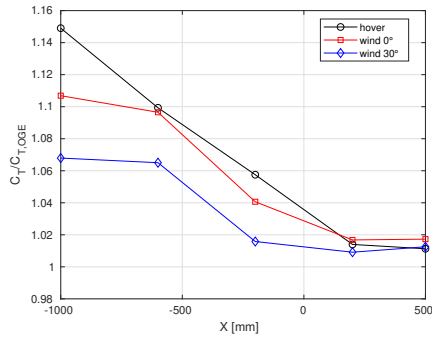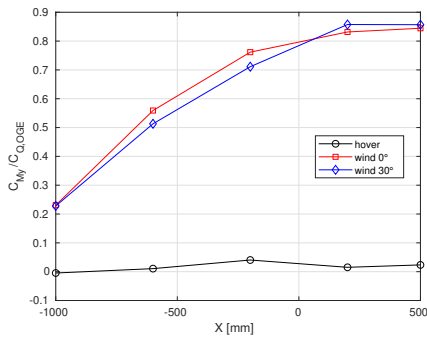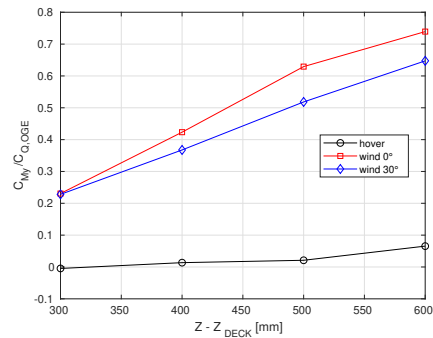
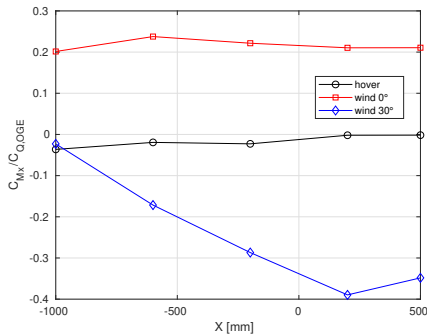(a) Thrust coefficient, stern landing
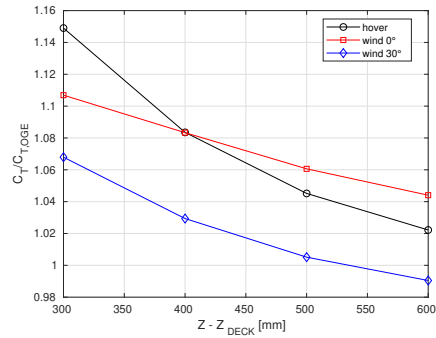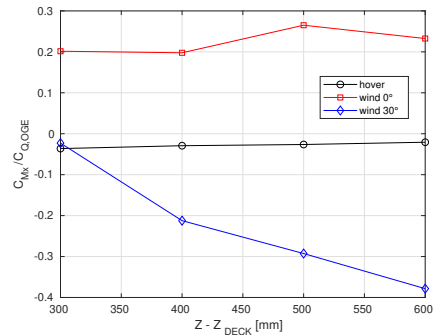
(b) Thrust coefficient, vertical landing

(c) Pitch moment coefficient, stern landing

(d) Pitch moment coefficient, vertical landing

(e) Roll moment coefficient, stern landing

(f) Roll moment coefficient, vertical landing

Figure 12 – Loads acting on the rotor: comparison of stern landing (left) and vertical descent (right), in three different test conditions:hover, headwind and R30 . On the left, going from right to left, the helicopter is moving from P1 to P5. On the right, going from right to left the helicopter is moving from P8 to P5.

4.3 Ship-Helicopter Interaction: Unsteady Measurements

As mentioned before, to measure the unsteady loads, first the rotor was trimmed at each position to obtain a constant thrust coefficient of 0.0028 and zero in-plane moments which could be achieved by applying collective and cyclic controls through the swashplate. Before unsteady analysis, the mean aerodynamic loads measured during 30 seconds of acquisition, are compared to verify that the trim objectives are respected. This comparison confirms that in all tests, the thrust was kept within the range of $\pm 10\%$ of the trim objective. For the roll and pitch moments, the value of $0 \pm 0.7 Nm$ was considered acceptable, that is 25% of the maximum moment obtained during no trim tests. Then, to quantify the unsteady aerodynamic loading of the rotor, same approach used for unsteady pressure has been implemented. In this method, proposed by Lee and Zan [6, 7], the square-root of the integral of the PSDs over the bandwidth of interest, so-called RMS loading, is considered as the measure of unsteadiness. Since the low-frequency content of the airwake, in the bandwidth of 0.2-2

Hz, directly impacts the workload of the pilot, the integral should be calculated over the equivalent full-scale bandwidth, which needs to be correctly mapped into the frequency scale of the test. Regarding the frequency scale of 1:4.75, the bandwidth of interest maps into the range of 0.95-9.5 Hz. It should be mentioned that all the PSD calculations are performed using non-dimensional load coefficients, so the RMS quantities are non-dimensional as well.

To compare the effect of wind direction, three test conditions are selected with the same free stream velocity but from different directions: HW, R30, and R60. Figure 13 compares this effect on the RMS values of three load coefficients, for all test points along the stern trajectory and vertical offset.

(a) Thrust Coefficient

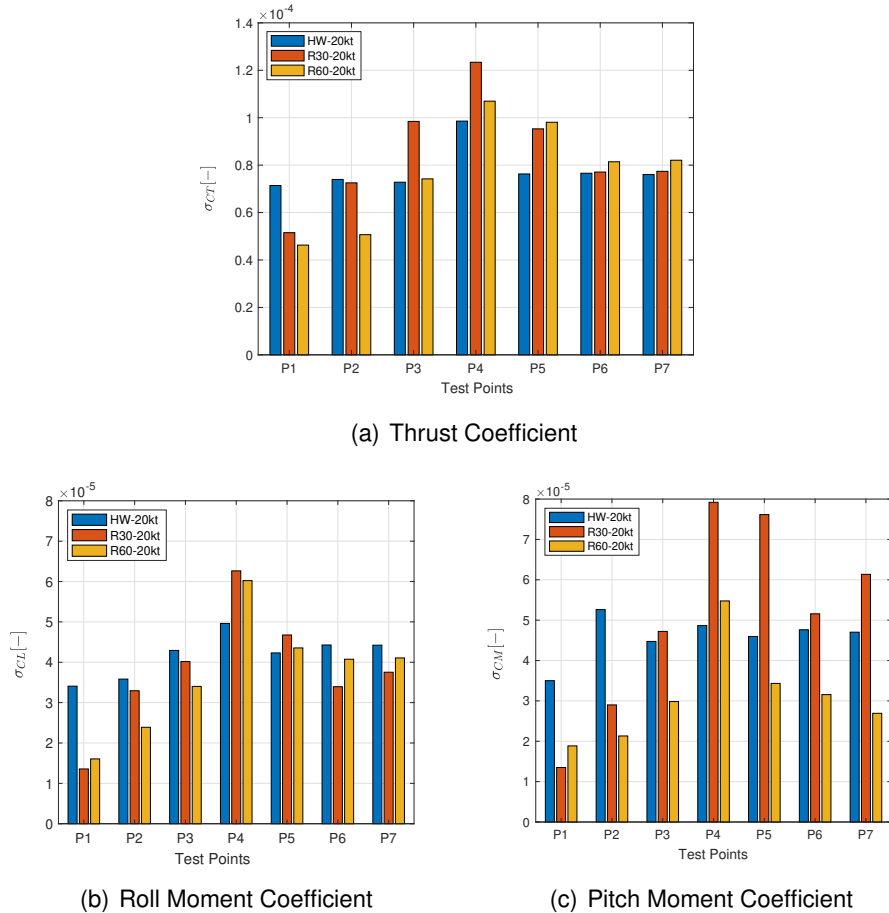(b) Roll Moment Coefficient

(c) Pitch Moment Coefficient

Figure 13 – Effect of wind direction on unsteady load coefficients, comparison of HW, R30 and R60.

Figure 13(a) shows that in all three wind directions, the unsteadiness of thrust is increased while moving towards the landing point, where the maximum unsteadiness is experienced at P4, with 38%, 240%, and 231% increase with respect to P1 in HW, R30, and R60 respectively. Moving upward from this point, the unsteadiness is reduced in all wind conditions. This trend can be explained by looking at the topology of the flow field over the deck of the isolated SFS1, presented previously in Fig. 5. Regarding the height of the rotor at P4, which is about 60% of the hanger height, at this position the rotor is immersed in the wake of the superstructure, especially the fore part of the rotor is significantly affected by the downwash due to the recirculation zone. This effect is reduced when the rotor is placed higher than the height of the hangar wall which results in the reduction of the unsteadiness in the last three points along the vertical trajectory. As represented in Figs. 13(b) and 13(c), both roll and pitch moments follow the same trend as observed in thrust. However, some differences can be appreciated as well. In the HW test, moving along the vertical path (P4 to P7) both moments do not show a noticeable reduction in unsteadiness with respect to the landing point (P4). Furthermore, in the same wind condition, the pitch moment at P2 has the highest unsteadiness which could be related to the asymmetric ground effect at this point, as the rotor is placed exactly above the stern edge. Thus, fore part of the rotor disk, which is above the deck, is more affected by the ground vortices compared to the aft part. In R60, roll moment shows more unsteadiness compared with the

pitch axis in all test points over the flight deck. This can be related to the spatial distribution of the turbulence intensity over the rotor disk which becomes more asymmetric in advancing and retreating side when the wind-angle increases towards the port or starboard side. Consequently, it can be expected that more unsteadiness is involved in roll moment while testing in R60.

To compare the effect of wind speed, two free stream velocities in headwind are selected. Figure 14 shows the variation of unsteadiness in aerodynamic loads, while free stream velocity is increased from 20 kt to 35 kt.

(a) Thrust Coefficient

(b) Roll Moment Coefficient
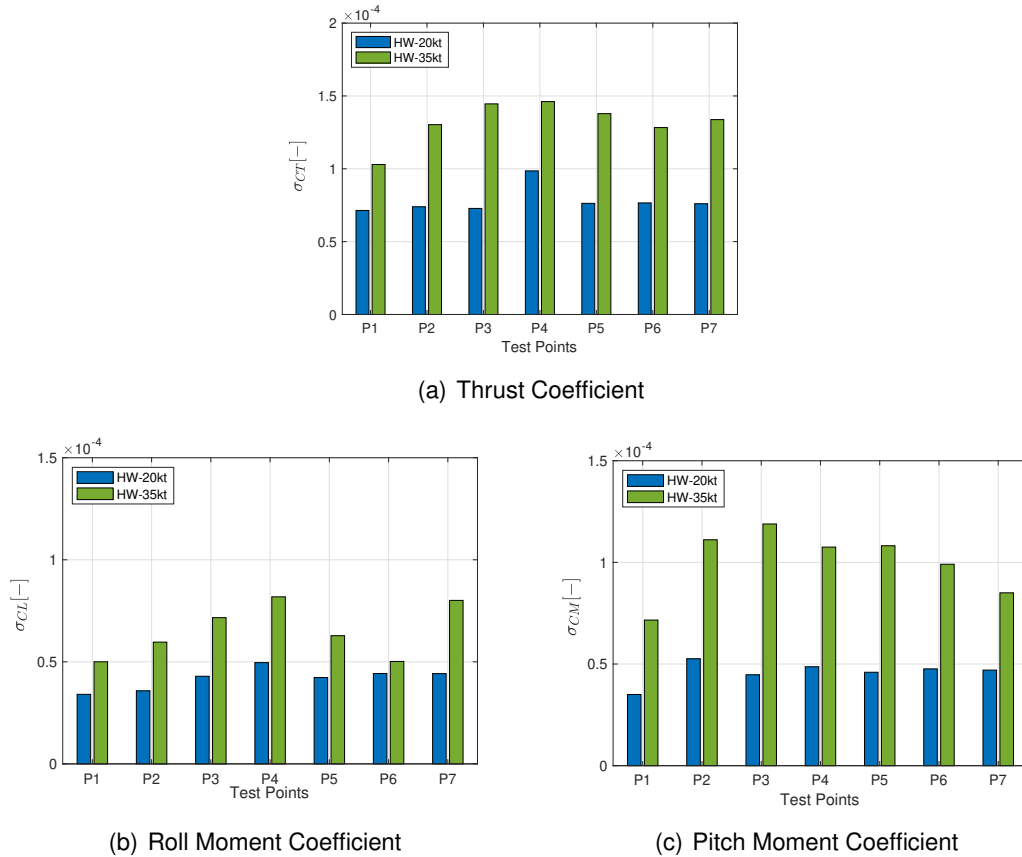
(c) Pitch Moment Coefficient

Figure 14 – Effect of wind speed on the unsteady load coefficients in HW test condition.

It should be noted that despite trimming the rotor in both wind speeds to obtain the same loads, the RMS values are increased in all three axes. For instance, a difference of 3% was observed in the mean value of trimmed thrust coefficient at P1, while the increase of unsteadiness is 44%, as represented in Fig. 14(a). Figure 14 shows that the unsteadiness of thrust, roll, and pitch moments are increased in all test points. However, the initial point, P1, is less affected compared with those which are over the deck. The strong coupling between inflow of the rotor and airwake of the ship at these points results in a more turbulent flow field which reflects in a notable increase of RMS loading. Regarding the moments, as expected the pitch moment is more amplified with respect to the lateral one. In addition to the HW condition and lateral symmetry of the SFS1 geometry, variation of the moments unsteadiness could be also related to the stronger coupling between average and longitudinal inflow state of the rotor, so that the unsteadiness in thrust will affect the pitch moment more than the lateral one.

The last set of RMS values is presented in Fig. 15 to see the effect of the dynamic approach on the unsteady loads. The total acquisition of 30 seconds is used to calculate the PSD of the measured loads, so that the RMS loading can be compared with the previous measurements at each point. To maintain the same trim objective as previous tests, the required trim controls in static tests were linearly combined to obtain the time history of the collective and cyclic commands during the dynamic approach. In this way, the trim condition of the rotor remains the same as the static tests and the effect of approach velocity can be evaluated on the unsteady loads.

(a) Thrust Coefficient

(b) Roll Moment Coefficient
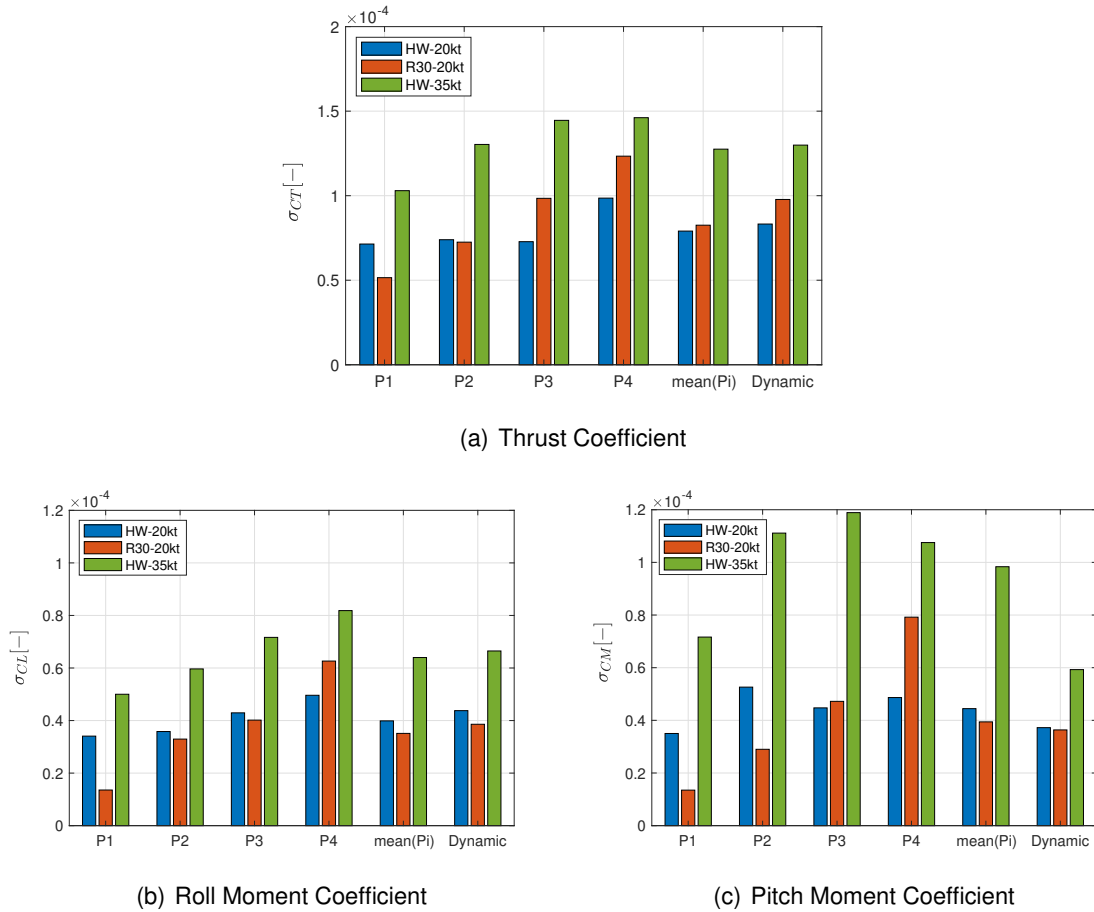

(c) Pitch Moment Coefficient

Figure 15 – Effect of approach velocity on the unsteady loading, comparison of static and dynamic tests.

Figure 15 shows the unsteady loading of the dynamic approach in comparison with the other 4 points of the trajectory. A weighted average of the unsteadiness obtained at each point has been calculated based on the fractions of total time spent between these four points. To have a better comparison with the dynamic test, this mean value is also presented in the fifth column. It can be seen that the weighted average of the unsteady thrust in both headwind tests represents a fairly good correlation with the dynamic approach, as they both remain in a range of $\pm 10\%$ from the unsteadiness measured in the dynamic approach, while in R30 the average of static measurements shows 15% less unsteadiness compared to the dynamic test. Regarding the in-plane moments, the unsteadiness of the roll moment in static and dynamic tests are very well correlated with less than 10% difference in all three wind directions. However, regarding the pitch moment, the averaged unsteadiness is higher than the one experienced during the dynamic test, especially in the headwind. Referring to Fig. 15(c), 8% and 19% differences can be observed in R30 and HW, where the wind speed is relatively low, while the difference is significantly increased to 67% for the HW test with the higher speed. These comparisons indicate that the approach velocity positively reduces the unsteady pitching moment experienced by the rotor during the landing maneuver. Consequently, it can be inferred that using the static approach to obtain the operational limits through simulation may result in a higher workload for the pilot and a more conservative envelope compared to the flight test.

5. Conclusion

This paper presents an experimental study of the aerodynamic interaction between a scaled-down helicopter model and the Simple Frigate Shape 1. A series of wind tunnel experiments was designed and carried out at the large test chamber of GVPM to investigate both the isolated-ship airwake and the effect of a fully coupled interaction on the aerodynamic loads of a scaled helicopter model while operating over the deck of SFS1. In the first part, pressure measurement and Particle Image

Velocimetry were performed to study the flow field over the deck of the isolated-SFS1 with respect to the three parameters: wind velocity, wind direction and presence of a turbulent Atmospheric Boundary Layer. The results showed that, within the range of tested free stream velocity, increasing the wind speed does not affect the structure of the flow field, while changing the wind direction, will significantly affect the size of the recirculation zone and its extension over the deck. It was also found the presence of the turbulent ABL increases the unsteadiness of the flow field which was more notable in Red30 wind condition and in the area closer to the stern side of the deck. Then, a scaled helicopter model was placed in a series of points representative of a stern landing trajectory and a vertical descent above the landing spot. While having a fixed pitch angle in all test positions, the time-averaged aerodynamic loads of the rotor were measured at each position. The ground effect of the deck was notable as the thrust increased in the positions closer to the surface of the deck. This effect was reduced in wind-on tests, especially when the wind was blowing from the port side of the deck. Another notable effect was reduction of the pitch moment along the stern landing and vertical descent trajectory, in both headwind and Red30 wind conditions.

In the next test campaign, the helicopter model was modified by implementing a swashplate mechanism so that the aerodynamic loads could be trimmed by applying collective and cyclic commands. Here, both time-averaged and unsteady loads of the rotor were measured for a range of wind velocity, direction and rotor position over the deck. Due to the trimming capability all ranges were increased with respect to the previous tests. At each position the rotor was trimmed in order to obtain a specific level of thrust and zero in-plane moments. The variation of unsteady thrust and roll moment along the landing trajectory showed that in all wind conditions, the highest unsteadiness is experienced by the rotor at the lowest altitude and closest position to the hangar wall. Regarding the pitch moment in headwind, a slightly different trend was observed, as the unsteadiness remained relatively high in all the points over the deck. Furthermore, the variation of unsteadiness with wind speed was found to be affected by the interaction of the rotor inflow and ship airwake. Consequently, the rate of increment was changed at different points along the landing path. Moreover, the effect of approach velocity on the unsteady loads was examined by performing a dynamic landing maneuver. Comparing the unsteadiness of dynamic tests with the measurements at fixed positions, confirmed a reasonable correlation in unsteady thrust and roll moment between two approaches. However, the unsteady pitch moment was found to decrease in dynamic landing. The reduction was especially notable while testing in headwind conditions and with higher wind speed. Consequently, assessment of the operational limits in DI simulation, based on the results of static approach may lead to over estimation of the pilot workload and impose unrealistic restrictions on the safe envelope of the operation.

6. Contact Author Email Address

Corresponding author: Neda.Taymourtash@polimi.it
Authors' contact:
Alex.Zanotti@polimi.it; Giuseppe.Gibertini@polimi.it; Giuseppe.Quaranta@polimi.it

7. Copyright Statement

8. Acknowledgment

References

[1] BARDERA-MORA, R., CONESA, A., AND LOZANO, I. Simple frigate shape plasma flow control. *Proceedings of the Institution of Mechanical Engineers, Part G: Journal of Aerospace Engineering 230*, 14 (2016), 2693–2699.

[2] BUCHHOLZ, J. H. J., MARTIN, J. E., KREBILL, A. F., DOOLEY, G. M., AND CARRICA, P. M. Structure of a ship airwake at model and full scale. In *54th AIAA Aerospace Sciences Meeting* (Kissimmee, Florida, January 2016).

[3] HOENCAMP, L. A., AND PAVEL, M. D. Concept of a predictive tool for ship–helicopter operational limitations of various in-service conditions. *Journal of the American Helicopter Society 57*, 3 (2012), 1–9.

[4] KÄÄRIÄ, C. H., WANG, Y., PADFIELD, G. D., FORREST, J. S., AND OWEN, I. Aerodynamic loading characteristics of a model-scale helicopter in a ship's airwake. *Journal of Aircraft 49*, 5 (2012), 1271–1278.

[5] KÄÄRIÄ, C. H., WANG, Y., WHITE, M. D., AND OWEN, I. An experimental technique for evaluating the aerodynamic impact of ship superstructures on helicopter operations. *Ocean Engineering 115* (2021).

[6] LEE, R. G., AND ZAN, S. J. Unsteady aerodynamic loading on a helicopter fuselage in a ship airwake. *Journal of the American Helicopter Society 49*, 2 (2004), 149–159.

[7] LEE, R. G., AND ZAN, S. J. Wind tunnel testing of a helicopter fuselage and rotor in a ship airwake. *Journal of the American Helicopter Society 50*, 4 (2005), 326–337.

[8] LI, T., WANG, Y., AND ZHAO, N. Numerical study of the flow over the modified simple frigate shape. *Proceedings of the Institution of Mechanical Engineers, Part G: Journal of Aerospace Engineering* (2020).

[9] LUMSDEN, B., WILKINSON, C. H., AND PADFIELD, G. D. Challenges at the helicopter-ship dynamic interface. In *24th European Rotorcraft Forum* (Sept. 1998).

[10] MARTINUZZI, R., AND TROPEA, C. The flow around surface-mounted, prismatic obstacles placed in a fully developed channel flow. *Transactions-American Society of Mechanical Engineers Journal of Fluids Engineering 115* (1993), 85–85.

[11] ROPER, D. M., OWEN, I., PADFIELD, G. D., AND HODGE, S. J. Integrating cfd and piloted simulation to quantify ship-helicopter operating limits. *The Aeronautical Journal 110*, 1109 (2006), 419–428.

[12] ROSENFIELD, N. C., KIMMEL, K. R., AND SYDNEY, A. J. Investigation of ship topside modeling practices for wind tunnel experiments. In *53rd AIAA Aerospace Sciences Meeting* (Kissimmee, Florida, January 2015).

[13] SIMIU, E., AND SCANLAN, R. H. *Wind Effect on Structures Fundamentals and Applications to Design*, third ed. John Wiley and Sons Inc., 1986, ch. 2, p. 46.

[14] SYMS, G. F. Simulation of simplified-frigate airwakes using a lattice-boltzmann method. *Journal of Wind Engineering and Industrial Aerodynamics 96*, 6-7 (2008), 1197–1206.

[15] TAYMOURTASH, N., ZAGAGLIA, D., ZANOTTI, A., MUSCARELLO, V., GIBERTINI, G., AND QUARANTA, G. Experimental study of a helicopter model in shipboard operations. *Aerospace Science and Technology 61* (2013), 97–108.

[16] TAYMOURTASH, N., ZANOTTI, A., GIBERTINI, G., AND QUARANTA, G. Unsteady load assessment of a scaled-helicopter model in a ship airwake. *Aerospace Science and Technology In press* (2022).

[17] WANG, Y., CURRAN, J., PADFIELD, G. D., AND OWEN, I. Airdyn: an instrumented model-scale helicopter for measuring unsteady aerodynamic loading in airwakes. *Measurement Science and Technology 22*, 4 (2011), 045901.

[18] WELCH, P. D. The use of fast fourier transform for the estimation of power spectra: A method based on time averaging over short, modified periodograms. *IEEE Transactions on Audio and Electroacoustics 15*, 2 (1967), 70–73.

[19] WILKINSON, C., ZAN, S. J., GILBERT, N. E., AND FUNK, J. D. Modelling and simulation of ship air wakes for helicopter operations : A collaborative venture. In *AGARD Symposium on Fluid Dynamics Problems of Vehicles Operating near or in the Air-Sea Interface* (Amsterdam, The Netherlands, 1999).

[20] ZAGAGLIA, D., GIUNI, M., AND GREEN, R. B. Investigation of the rotor–obstacle aerodynamic interaction in hovering flight. *Journal of the American Helicopter Society 63*, 3 (2018), 1–12.

[21] ZAN, S. Surface flow topology for a simple frigate shape. *Canadian Aeronautics and Space Journal 47*, 1 (2001), 33–43.

[22] ZAN, S. J., SYMS, G. F., AND CHENEY, B. T. Analysis of patrol frigate air wakes. In *RTO AVT Symposium on "Fluid Dynamic Problems of Vehicles Operating near or in the Air-Sea Interface"* (1998).